Transition from vortices to solitonic vortices in trapped atomic Bose-Einstein condensates

M. C. Tsatsos,[1,*] M. J. Edmonds,[2] and N. G. Parker[2]

[1]*São Carlos Institute of Physics, University of São Paulo, P.O. Box 369, 13560-970 São Carlos, São Paulo, Brazil*

[2]*Joint Quantum Centre (JQC) Durham-Newcastle, School of Mathematics and Statistics, Newcastle University, Newcastle upon Tyne NE1 7RU, United Kingdom*

(Received 17 March 2016; published 24 August 2016)

Motivated by recent experiments, we study theoretically the dynamics of vortices in the crossover from two dimensions to one in atomic condensates in elongated traps. We explore the transition from the dynamics of a vortex to that of a dark soliton as the one-dimensional limit is approached, mapping this transition out as a function of the key system parameters. Moreover, we probe this transition dynamically through the hysteresis under time-dependent deformation of the trap at the dimensionality crossover. When the solitonic regime is probed during the hysteresis, significant angular momentum is lost from the system, but remarkably, the vortex can reemerge.

DOI: 10.1103/PhysRevA.94.023627

I. INTRODUCTION

Atomic Bose-Einstein condensates (BECs) provide rich insight into superfluidity, buoyed by their purity and immense ability to control and image the coherent matter wave [1]. Of particular interest are coherent macroscopic excitations in the form of quantized vortices [2,3] and dark solitons [4]. Quantized vortices represent defects in the quantum-mechanical phase about which the superfluid flows with quantized circulation and appear pointlike in two dimensions and as vortex lines or rings in three dimensions. Early landmark demonstrations of single vortices [5,6], vortex arrays and lattices [7–9], and vortex rings [10] have been supplemented more recently by the deterministic generation of vortex dipoles [11,12], real-time observation of vortex dynamics [13], and turbulent states of disordered vortices [14–16]. Meanwhile, atomic dark solitons are one-dimensional (1D), nondispersive matter waves characterized by a notch in the atomic density and a nontrivial phase slip [4,17]. They are favored under repulsive *s*-wave atomic interactions, which give rise to the required defocusing mean-field nonlinearity. Experiments have controllably generated dark solitons [18–26], including long-lived solitons at ultralow temperatures in tightly 1D geometries [23], and studied their oscillations, interactions, and collisions [23,25,26].

Dark solitons and vortices are formally distinct objects with differing dimensionalities and topological properties; vortices can only disappear at a boundary or by annihilating with an opposite-circulation vortex, while dark solitons have no such constraint. In a harmonic trap, a dark soliton tends to oscillate axially at a fixed proportion of the trap frequency [27–30], while a vortex precesses about the trap center at a frequency with a nontrivial dependence on its position and system parameters [31–35]. Remarkably, however, dark solitons and vortices show many analogous behaviors, underpinned by their common nature as phase defects, such as their spontaneous creation under the Kibble-Zurek mechanism [36–38], their emergence during the breakdown of superflow [11,16,22,39–41], their instability to acceleration [42,43], and their interaction with phonons [44,45].

The intimate connection between vortices and dark solitons is perhaps best revealed at the dimensionality crossover. While dark solitons are dimensionally stable in quasi-1D geometries [46], three-dimensional (3D) dark solitons are unstable to transverse perturbations; the nodal line undergoes the *snake instability* (known from earlier studies in optics [47]) and decays into one or more vortex rings (or vortex-antivortex pairs in two dimensions) [10,20,48,49]. Close to the 1D boundary, hybrid dark-soliton–vortex-ring excitations have been observed [50]. Theoretical analysis of the possible solutions confirmed this behavior but also predicted the existence of solitonic vortex solutions [51–53], that is, a single vortex confined to move along the long axis. This excitation is predicted to be favored when the transverse size is large enough to make the dark soliton unstable but not so large as to support vortex rings. In recent experiments these solitonic vortices have been reported in both Bose [54,55] and Fermi gases [56]. Moreover, recent theoretical work has shown that solitonic vortices are part of a larger family of higher-energy solitary wave defects termed Chladni solitons [57].

Motivated by these recent experiments, we examine the crossover from vortices to solitonic vortices in trapped condensates. Based on numerical simulations of the 2D Gross-Pitaevskii (GP) equation, we investigate the propagation of the vortex and solitonic vortex in static traps with differing aspect ratios. We map out how the oscillation frequency of the excitation changes with the trap ratio; as the latter increases, the oscillation frequency saturates to that expected for a dark soliton, marking the onset of the solitonic vortex regime. This occurs when the transverse harmonic oscillator length becomes roughly equal to twice the healing length (the characteristic size of the vortex). While the transition from a dark soliton to a solitonic vortex has also been mapped out numerically in Ref. [53] in terms of the excitation density profile, here we focus on the dynamical behavior of the wave through its oscillation frequency, a quantity which can be accurately measured experimentally (to within a few percent) using real-time vortex imaging [13]. Furthermore, we examine the dynamics in traps with a time-dependent trap ratio, exploring the hysteresis across the vortex–solitonic-vortex crossover. We find that observable deviations of the angular momentum from

[*]Corresponding author: marios@ifsc.usp.br

its initial value can occur if the vortex–solitonic-vortex limit is crossed.

II. THEORETICAL MODEL

We consider a weakly interacting BEC at zero temperature composed of atoms of mass m and confined by a harmonic potential $V(x,y,z) = \frac{1}{2}m(\omega_x^2 x^2 + \omega_y^2 y^2 + \omega_z^2 z^2)$, where $\omega_{x,y,z}$ are the trap frequencies in the respective directions. The atomic interactions are modeled by the contact pseudopotential $g_0\delta(\mathrm{r}-\mathrm{r}')$, where $g_0 = 4\pi\hbar^2 a_s/m$ and a_s is the atomic s-wave scattering length. For simplicity we adopt a 2D model. The trapping along z is assumed to be sufficiently strong to render the condensate dynamics as quasi-two-dimensional [58]. Then, the two-dimensional (2D) condensate wave function $\psi(x,y,t)$ (normalized to the total particle number N) satisfies the effective 2D GP equation

$$i\hbar\frac{\partial\psi}{\partial t} = \left[-\frac{\hbar^2}{2m}\nabla^2 + V(x,y,t) + \frac{g_0}{\sqrt{2\pi}l_z}|\psi|^2\right]\psi, \qquad (1)$$

where $l_z = \sqrt{\hbar/m\omega_z}$ is the harmonic oscillator length along z. The energy scale of the condensate is characterized by the chemical potential μ, the eigenvalue associated with the Hamiltonian in Eq. (1). We present length, time, and energy in units of $l_x = \sqrt{\hbar/m\omega_x}$, ω_x^{-1}, and $\hbar\omega_x$, respectively. We quantify the atomic interactions by the dimensionless parameter $g = mNg_0/\sqrt{2\pi}\hbar^2 l_z$. After obtaining the vortex-free condensate solution [time-independent solution to Eq. (1)], a vortex is imposed, and the subsequent dynamics are simulated by numerical integration of the GP equation (further details are given in the Appendix). For a cigar-shaped geometry, we note that it is possible to describe the condensate featuring a vortex through a 1D nonpolynomial Schrödinger equation [59].

III. RESULTS: EVOLUTION FOR VARIOUS ASPECT RATIOS

To illustrate the crossover from vortices to solitonic vortices, we show the condensate evolution (density and phase) in Fig. 1 under three different trap ratios, with the vortex initially at $(x_{V,0},y_{V,0}) = (1.5l_x,0)$. For a circular trap ($\omega_y/\omega_x = 1$) and a weakly elongated trap ($\omega_y/\omega_x = 4$), the vortex precesses in circular and elliptical paths, respectively. This is to be expected since, in the absence of thermal dissipation, vortices follow equipotential trajectories [60], which can be understood in terms of the Magnus force acting on the vortex due to the inhomogeneous density. The vortex maintains a circular core and a 2π corkscrew phase profile. For considerably higher trap ratio ($\omega_y/\omega_x = 15$), however, the initially imprinted vortex rapidly deforms into a stripelike density depression, and the phase profile becomes more steplike (with a rapid variation at the poles and almost uniform at the sides). As we will show, this structure behaves as a solitonic vortex.

To assess how vortexlike or solitonlike the dynamics of the excitation is, we monitor its oscillation frequency ω_V. The excitation's trajectory $\{x_V(t),y_V(t)\}$ is tracked according to its density minimum [61]; ω_V is determined from the Fourier frequency spectrum of $x_V(t)$. A single vortex is predicted to precess with a relatively small frequency which

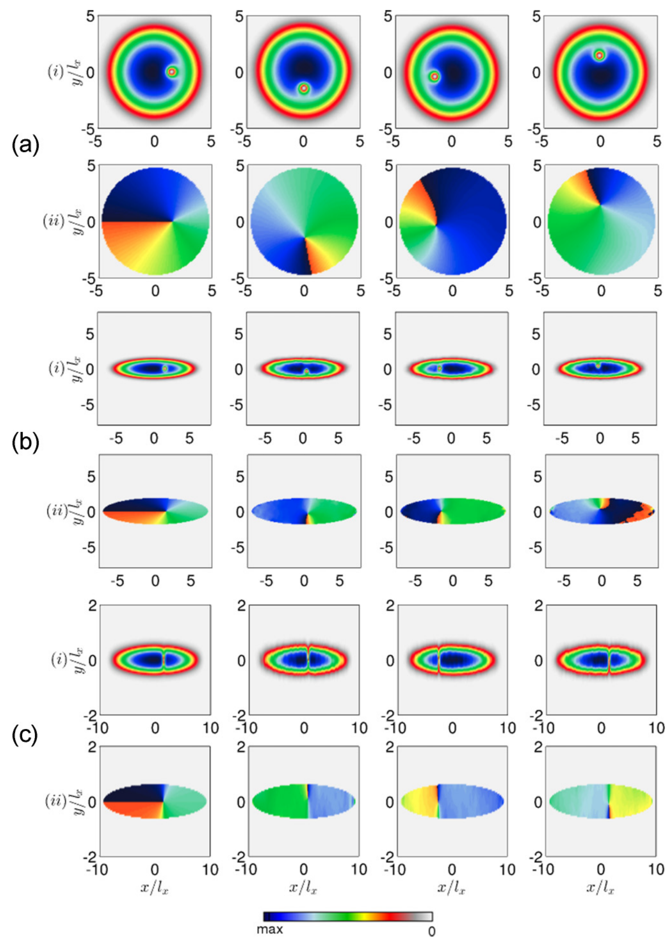

FIG. 1. Evolution of the condensate (i) density and (ii) phase profiles for trap ratios (a) $\omega_y/\omega_x = 1$, (b) 4, and (c) 15. We take $g = 400$ and the vortex initial position $(x_{V,0},y_{V,0}) = (1.5l_x,0)$. From left to right the columns represent $t = 0$, $T_V/4$, $T_V/2$, and $3T_V/4$, where $T_V = 2\pi/\omega_V$ is the vortex precession period [calculated from Eq. (4)]. All units are dimensionless.

depends nontrivially on its position, the trap frequencies, and the atomic interactions [62], as predicted using asymptotic expansions [31,32] and variational techniques [33,34]. Meanwhile, for a 1D condensate in the Thomas-Fermi (TF) limit ($Na_s/l_x \gg 1$), a dark soliton is expected to oscillate at a frequency $\omega_S = \omega_x/\sqrt{2}$ [27–30]. Figure 2(a) plots ω_V measured across multiple simulations with varying trap ratio. For each interaction strength g considered, ω_V is seen to increase with the trap ratio ω_y/ω_x, saturating at a value close to the expected dark-soliton frequency $\omega_S = \omega_x/\sqrt{2}$ (blue dashed line). This demonstrates the solitonlike behavior of the excitation for sufficiently high trap ratios. Note that ω_V does not exactly tend to $\omega_x/\sqrt{2}$; this prediction assumes the one-dimensional and TF limits. Away from these limits the soliton frequency can deviate by up to 10% [46], consistent with our observations.

It is evident from Fig. 2(a) that, for higher g values, the solitonic limit requires higher trap ratios. It is expected that the solitonic (quasi-1D) limit is reached when the transverse size of the system becomes of the order of the healing length, $\xi = \hbar/\sqrt{2mg}$, which characterizes the size of the vortex [51]. Since

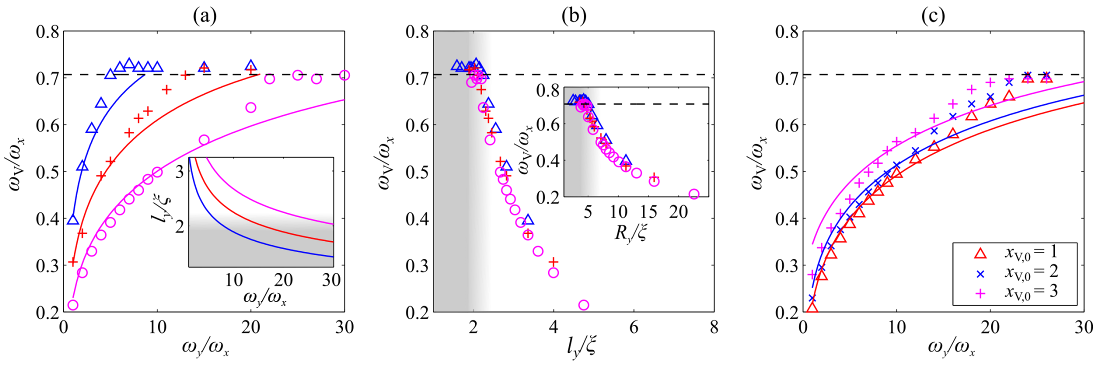

FIG. 2. (a) Vortex and solitonic vortex oscillation frequency ω_V versus trap ratio ω_y/ω_x for interaction strengths $g = 100$ (blue triangles), 200 (red crosses) and 400 (magenta circles), according to simulations (markers) and Eq. (4) (lines). The inset shows the relationship between l_y/ξ and the trap ratio. The vortex is started at $(x_{V,0},y_{V,0}) = (1.5l_x,0)$. Shading indicates the solitonic regime. (b) As in (a) but with ω_V plotted versus l_y/ξ and also versus R_y/ξ (inset). (c) Oscillation frequency versus trap ratio for different initial positions $x_{V,0}$ as per the legend (and $g = 400$). The black dashed lines indicate the predicted soliton frequency $\omega_S = \omega_x/\sqrt{2}$. All units are dimensionless.

the healing length scales as $1/\sqrt{g}$, for larger values of g tighter confinement in y is required to reach this limit. We formalize this criterion as follows. In the TF approximation, density gradients are neglected, and the resulting density from Eq. (1) takes the form $n(x,y) = n_0(1 - x^2/R_x^2 - y^2/R_y^2)$, where n_0 is the central (2D) density and $R_{x,y}^2 = 2\mu/m\omega_{x,y}^2$ define the TF radii in the respective directions. Applying the normalization $N = \int n(x,y)dxdy$ leads to

$$\mu = \hbar\omega_x\sqrt{2\sqrt{\frac{2}{\pi}}\frac{a_s N}{l_z}\frac{\omega_y}{\omega_x}}. \tag{2}$$

Then, the ratio of the transverse harmonic oscillator length $l_y = \sqrt{\hbar/m\omega_y}$ (which characterizes the transverse condensate width) to the healing length ξ follows as

$$\frac{l_y}{\xi} = \sqrt{\frac{2\mu}{\hbar\omega_y}} = \left(\frac{4g\omega_x}{\pi\omega_y}\right)^{1/4}. \tag{3}$$

This is plotted as a function of the trap ratio in Fig. 2(a) (inset). Upon plotting the oscillation frequency ω_V as a function of l_y/ξ (rather than trap ratio), the data fall onto a common curve [Fig. 2(b)]. Moreover, the solitonic limit is commonly reached when $l_y/\xi \lesssim 2$ (shaded region). One may instead define the transverse condensate as the scaled TF radius R_y/ξ [inset of Fig. 2(b)]; again, the data fall onto a common universal curve, with the solitonic limit reached for $R_y/\xi \lesssim 5$ (shaded region). The transition between a dark soliton and a solitonic vortex has also been mapped theoretically in Ref. [53], also revealing a universal behavior as a function of trap ratio; however, there the transition was mapped out in terms of the density profile of the excitation, rather than the dynamical characterization herein in terms of its oscillation frequency.

In the 2D regime ($l_y/\xi \gg 2$) the excitation should behave as a true 2D vortex. Using a variational Lagrangian method in the TF limit, Kim and Fetter [62] predicted elliptical vortex trajectories under nonaxisymmetric 2D harmonic confinement, governed by the equations $\dot{x}_V(t) = -(\omega_y/\omega_x)\omega_V y_V(t)$ and $\dot{y}_V(t) = (\omega_x/\omega_y)\omega_V x_V(t)$, where the precession frequency ω_V of the vortex is defined as

$$\omega_V = \frac{3}{2}\frac{\hbar}{mR_xR_y}\ln\left(\frac{R_\perp}{\xi}\right)\frac{1}{1-r_0^2}, \tag{4}$$

with $R_\perp^2 = 2R_x^2R_y^2/(R_x^2 + R_y^2)$ and r_0 being the radial coordinate of the vortex scaled in TF units, i.e., $r_0^2 = (x_{V,0}/R_x)^2 + (y_{V,0}/R_y)^2$. This agrees well with vortex precession frequencies measured experimentally [63] for a vortex line in an elongated 3D condensate. It also agrees well with the present simulated vortex dynamics up to moderate trap ratios, beyond which ω_V is underestimated [solid lines, Fig. 2(a)]. This difference is likely due to both the deviation from a TF state as the trap ratio increases and also the breakdown of the assumption of a vortex phase profile used for the variational ansatz that underlies Eq. (4).

Figure 2(c) shows the oscillation frequency for different initial vortex positions, $x_{V,0} = \{1,2,3\}l_x$, at fixed interaction strength, $g = 400$ (for comparison, $R_x \approx 5l_x$). The data have a similar behavior for all three positions, with the curves shifting up slightly compared to the prediction of Eq. (4) for increasing $x_{V,0}$. The solitonic limit is reached at a similar trap ratio, $\omega_y/\omega_x \approx 20$. Good agreement with Eq. (4) is found for vortices placed close to the trap center. The agreement worsens for vortices placed off center. This is to be expected since off-center vortices probe more of the non-TF tails of the condensate. Importantly, the insensitivity of the solitonic limit to the vortex position underpins the primary role of the condensate aspect ratio (quantified via l_y/ξ or R_y/ξ in this work) in controlling the effective dimensionality of the excitation.

IV. RESULTS: EVOLUTION UNDER TRAP DEFORMATION

We now turn our attention to the fate of the vortex in a trap that is dynamically deformed from an initially axisymmetric geometry to a highly elongated (along x) one and back again, seeking to address the persistence of the vortex and the hysteresis of the system. ω_y is made time dependent so as to evolve the trap ratio $\omega_y(t)/\omega_x$ as per Fig. 3(a): after an initial wait ($t_1 = 16\omega_x^{-1}$, approximately one vortex precession

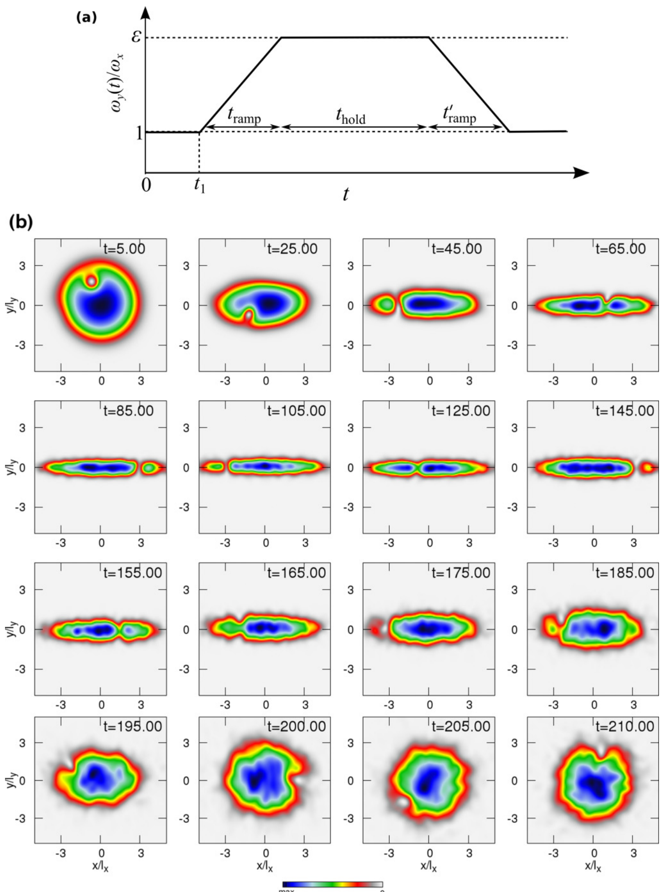

FIG. 3. Dynamics under the trap deformation. (a) The imposed time-dependent deformation of the trap ratio. (b) Evolution of the condensate density during a hysteresis protocol from axisymmetric to elongated and back again. Here $g = 100$, $(x_{V,0}, y_{V,0}) = (1.5, 0)l_x$, $\varepsilon = 8$, $t_{\rm ramp} = 70\omega_x^{-1}$, and $t_{\rm hold} = 40\omega_x^{-1}$. All units are dimensionless.

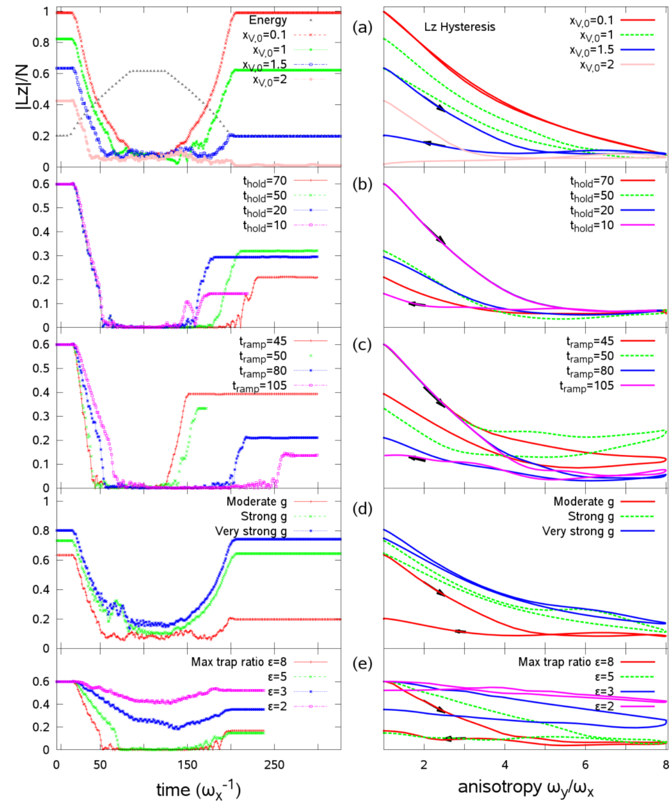

FIG. 4. Angular momentum per particle L_z versus time (left) and trap ratio ω_y/ω_x (right). From (a) to (e) we show the cases for different initial vortex positions, hold times, ramp times, interaction strengths, and maximum trap anisotropies. For the $|L_z(\omega_y/\omega_x)|$ hysteresis plots the data are smoothed with Bézier curves. Unless varied, the parameter values are $g = 100$, $t_{\rm ramp} = 70\omega_x^{-1}$, $t_{\rm hold} = 40\omega_x^{-1}$ $x_{V,0} = 1.5l_x$, and $\varepsilon = 8$. The gray triangles (here out of scale) in the top left panel show the relative increase of the total energy of the system $E/E(t = 0)$ that grows as large as 3. See text for details. All units are dimensionless.

period for $g = 100$), the trap ratio is ramped linearly to a maximum value ε over time $t_{\rm ramp}$, held there for $t_{\rm hold}$, and then linearly reduced back to an axisymmetric trap over $t_{\rm ramp}$. We note that such a time-dependent variation of the trap ratio could be achieved in the laboratory using an optical atomic trap where the applied beam waists are gradually modulated in time (see, for instance, [64]). Taking, for example, a typical trap frequency $\omega_x = 2\pi \times 20$ Hz, our time unit ω_x^{-1} is 8 ms. Then the time scales we consider for the ramping and holding of the deformation, which are of the order of 10–100ω_x^{-1}, correspond to the order of 80–800 ms. These time scales are realistic to achieve, being long enough to comfortably modulate the optical field while staying well within the lifetimes of typical condensates (a few seconds).

An example case, with maximum trap ratio $\varepsilon = 8$ and $g = 100$, is shown in Fig. 3(b). By comparison to Fig. 2(a) it is evident that, for this maximum trap ratio, the system enters the solitonic regime. It is useful to characterize the system through its total angular momentum $L_z = -i\hbar\langle\psi|x\partial_y - y\partial_x|\psi\rangle$. The evolution of L_z for this system is shown in Fig. 4(a) (left column, pink line). As the trap ratio is increased, the precessing vortex deforms into a 1D-like solitonic vortex, which oscillates axially. During the increase of the trap ratio L_z decreases. Upon reducing the trap ratio, the vortex is remarkably seen to reemerge in the system, albeit with increased radial position. Concurrent with this, the angular momentum rises again, saturating at a value which is about one third of its initial value, consistent with the drift of the vortex to the edge. The time-dependent anisotropy of the system couples with the system's nonzero angular momentum L_z, resulting in a smaller value of $|L_z|$ than the initial one. The condensate also develops considerable surface excitations during the deformation process.

The gray dotted line [left panel of Fig. 3(a)] is the variation in the total energy of the system (energy at time t divided by the energy at equilibrium), here not to scale. In all cases studied, the total energy increased up to a value that follows $\sim\sqrt{\varepsilon}$ and then returned to a value marginally (∼0.2%–2%) higher than the initial one, thus making the whole process a nonviolent one. Since the vortex energy accounts only for 8%–10% of the total energy (depending on the vortex position), this comes as no surprise. We conclude that the hysteresis loop affects the angular momentum but not (significantly) the energy.

For an adiabatical deformation of the trap, L_z should depend only on the instantaneous trap ratio. It is clear here, however, that angular momentum is lost from the vortex during the dynamics, giving rise to a hysteresis effect. This is revealed by plotting a hysteresis curve of L_z versus trap ratio in Fig. 4(a) (right column, pink line); arrows denote the direction of time.

In all cases shown in Fig. 4 (right column), L_z systematically decreases with the trap ratio. We can qualitatively understand this behavior by the following simple model, an extension of the superfluid bucket model [65] from a circular cross section to an elliptical cross section. Consider, for simplicity, the condensate to be 2D and of uniform density n_0 within the Thomas-Fermi perimeter defined by the ellipse $(x/R_x)^2 + (y/R_y)^2 = 1$. Moreover, consider the condensate to feature a singly quantized vortex at the origin, about which the fluid velocity has the conventional radial dependence for a bulk quantized vortex of $v(r) = \hbar/mr$. Then, the angular momentum L_z of the condensate can be evaluated in this fluid picture as $L_z = \int mn(x,y)v(x,y)dxdy$, where the integral is performed across the condensate region, excluding the vortex core, which is assumed to be of negligible size. This leads to

$$L_z = \frac{\pi n_0 \hbar R_x^2}{\omega_y/\omega_x}. \tag{5}$$

While this model ignores effects from the inhomogeneous density, the vortex core, and the modification of the vortex due to the boundary, it nonetheless reveals the rudimentary coupling between the angular momentum and the trap ratio, with the angular momentum scaling with the inverse of the trap ratio. Moreover, as the vortex is moved away from the center of the condensate, the total angular momentum of the system decreases, as has been established for circular traps [66].

In general, the angular momentum does not return to its initial value at the end of the deformation cycle. The mechanisms behind this hysteresis are nontrivial and likely to involve effects including coupling to surface modes (whose spectra will themselves be time and dimensionality dependent), as well as emission and absorption of phonons by the defect. To shed light on the hysteresis we next make a systematic study of how the key physical parameters, vortex initial position, ramping rate, interactions, and maximum trap ratio, affect the final state of the vortex and its hysteresis. The results are shown in Figs. 4(a)–4(e). We vary each of these quantities in turn while keeping the remaining parameters fixed (with values stated in the figure caption).

(a) Vortex position. We consider four initial vortex positions, $x_{V,0} = \{0.1,1,1.5,2\}l_x$ and $y_{V,0} = 0$. For comparison, the (axisymmetric) TF radius is $R_x = 3.4l_x$. The loss in angular momentum increases for a vortex positioned away from the trap center. Indeed, for positions $\gtrsim 0.6R_x$, the remaining angular momentum is negligible, and the vortex is destroyed by the process. Conversely, for a vortex initially placed close to the trap center, the vortex remains intact, and the system recovers its original angular momentum and undergoes an almost time-symmetric hysteresis. We hypothesize that the fragility of vortices which are initially positioned close to the edge is due to enhanced coupling with surface modes of the condensate.

(b) Hold time. We fix $t_{\text{ramp}} = 70\omega_x^{-1}$ and investigate the impact of the hold time on the residual angular momentum (AM) by considering four different values ($t_{\text{hold}} = 10,20,50,70$). Note that the deformation cycles employed here and in the following are on time scales greater than the vortex periods. For the same initial value, the angular momentum drops at different rates. Even though the relationship of L_z with t_{hold} is not linear (compare $t_{\text{hold}} = 70$ with $t_{\text{hold}} = 50$), we have seen that the general tendency of increasing t_{hold} is to increase L_z.

(c) Ramp time. We now fix t_{hold} at $40\omega_x^{-1}$ and vary t_{ramp}. Slower deformation results in an increased loss in L_z. This is counterintuitive: as the deformation cycle slows down, one might expect the process to approach an adiabatic one and hence the hysteresis effect to vanish. We attribute the significant loss in angular momentum for slow deformations to an integrative, cumulative effect over time during the long deformation time scale. However, a full understanding of this behavior warrants further investigation.

(d) Interaction. For moderate interactions ($g = 100$), angular momentum is lost during the process, while for strong ($g = 200$) and very strong interactions ($g = 400$) almost no angular momentum is lost, and the hysteresis curve is time symmetric. This difference is attributed to the different dimensionalities probed: for moderate interactions this system crosses the border into the solitonic regime, while for the strong and very strong cases the system remains effectively 2D throughout. This is seen by comparison to Fig. 2(a).

(e) Maximum trap ratio. Last, we compare different maximum trap ratios, $\varepsilon = \{2,3,5,8\}$. For given interaction strength ($g = 100$) these values lie around the transition from two dimensions to the solitonic regime [see Fig. 2(a)], and it is not surprising that the loss in angular momentum becomes larger for larger values of ε, i.e., as the solitonic regime is increasingly entered.

V. CONCLUSIONS

We have explored the fate of vortices in highly elongated traps. We mapped out the transition from vortex to solitonic vortex in terms of its oscillation frequency, a particularly relevant quantity since it can be extracted experimentally with accuracy. The behavior of the oscillation frequency was characterized as a function of the key system parameters (trap anisotropy, interaction strength, and vortex position). The frequency increases with the anisotropy and approaches the value $\omega_S \approx \omega_x/\sqrt{2}$, characteristic of the dark soliton oscillation.

Depending on the ratio of the healing length to the oscillator length and the initial position (initial angular momentum), the solitonic vortex will survive a continuous deformation of the trap and reappear as a vortex once the symmetry of the trap is restored (see Fig. 3), although significant angular momentum can be lost if the solitonic regime is entered.

Deforming and resymmetrizing the trap that contains a solitonic vortex are an achievable way to probe physics in scales smaller than the healing length, currently considered inaccessible to experimentalists, and could assist in current research in quantum turbulence [67] where the participation of several length scales is required.

Last, we mention that beyond-mean-field descriptions have recently revealed how, in several cases, quantized vorticity concurs with nontrivial correlations and loss of coherence

[68–70]. It would be interesting to extend the present studies to fragmented condensates as well.

ACKNOWLEDGMENTS

M.C.T. acknowledges financial support from FAPESP and CePOF–Centro de Pesquisa em Óptica e Fotônica and computational time on Hornet/HazelHen facilities of the High Performance Computing Center Stuttgart (HLRS). A. U. J. Lode is thanked for developing numerical routines. We also thank P. G. Kevrekidis and P. E. S. Tavares for useful comments. M.J.E. and N.G.P. acknowledge support by EPSRC (UK) Grant No. EP/M005127/1.

APPENDIX

For the static trap simulations, the GP equation is evolved numerically using a Crank-Nicolson scheme on a spatial grid with typical spacing $\Delta x = 0.05 l_x$. The initial state $\psi_{\rm in}$ can be written using the Madelung transformation as $\psi_{\rm in} = \sqrt{n(x,y)}\exp[i\phi_V(x,y)]$, which is found by imaginary-time propagation of the GP equation [71] while enforcing a vortex phase defect at $\{x_{V,0},y_{V,0}\}$ using

$$\phi_{\rm V}(x,y) = \arctan\left(\frac{y-y_{V,0}}{x-x_{V,0}}\right). \tag{A1}$$

Meanwhile, for the time-dependent simulations, the initial state $\psi_{\rm in}$ is defined as

$$\psi_{\rm in} = \psi_{\rm back}\sqrt{\frac{X^2+Y^2}{X^2+Y^2+\delta}}\exp[i\phi_{\rm V}(x,y)], \tag{A2}$$

where $X = (x - x_{V,0})/\sigma_x, Y = (y - y_{V,0})/\sigma_y$, and $\psi_{\rm back}$ defines the vortex-free background state (found by imaginary-time propagation). The parameters δ,σ_x,σ_y, which determine the shape of the vortex, are determined by energy minimization. The system is evolved using the MCTDH-X package [72], taking $N = 100$ and $M = 1$.

[1] I. Bloch, J. Dalibard, and W. Zwerger, Rev. Mod. Phys. **80**, 885 (2008).
[2] A. L. Fetter, Rev. Mod. Phys. **81**, 647 (2009).
[3] B. P. Anderson, J. Low Temp. Phys. **161**, 574 (2010).
[4] D. J. Frantzeskakis, J. Phys. A **43**, 213001 (2010).
[5] M. R. Matthews, B. P. Anderson, P. C. Haljan, D. S. Hall, C. E. Wieman, and E. A. Cornell, Phys. Rev. Lett. **83**, 2498 (1999).
[6] P. Rosenbusch, V. Bretin, and J. Dalibard, Phys. Rev. Lett. **89**, 200403 (2002).
[7] K. W. Madison, F. Chevy, W. Wohlleben, and J. Dalibard, Phys. Rev. Lett. **84**, 806 (2000).
[8] J. R. Abo-Shaeer, C. Raman, J. M. Vogels, and W. Ketterle, Science **292**, 476 (2001).
[9] E. Hodby, G. Hechenblaikner, S. A. Hopkins, O. M. Marago, and C. J. Foot, Phys. Rev. Lett. **88**, 010405 (2001).
[10] B. P. Anderson, P. C. Haljan, C. A. Regal, D. L. Feder, L. A. Collins, C. W. Clark, and E. A. Cornell, Phys. Rev. Lett. **86**, 2926 (2001).
[11] T. W. Neely, E. C. Samson, A. S. Bradley, M. J. Davis, and B. P. Anderson, Phys. Rev. Lett. **104**, 160401 (2010).
[12] W. J. Kwon, S. W. Seo, and Y.-i. Shin, Phys. Rev. A **92**, 033613 (2015).
[13] D. V. Freilich, D. M. Bianchi, A. M. Kaufman, T. K. Langin, and D. S. Hall, Science **329**, 1182 (2010).
[14] E. A. L. Henn, J. A. Seman, G. Roati, K. M. F. Magalhães, and V. S. Bagnato, Phys. Rev. Lett. **103**, 045301 (2009).
[15] T. W. Neely, A. S. Bradley, E. C. Samson, S. J. Rooney, E. M. Wright, K. J. H. Law, R. Carretero-González, P. G. Kevrekidis, M. J. Davis, and B. P. Anderson, Phys. Rev. Lett. **111**, 235301 (2013).
[16] W. J. Kwon, G. Moon, J. Y. Choi, S. W. Seo, and Y. I. Shin, Phys. Rev. A **90**, 063627 (2014).
[17] W. P. Reinhardt and C. W. Clark, J. Phys. B **30**, L785 (1997).
[18] S. Burger, K. Bongs, S. Dettmer, W. Ertmer, K. Sengstock, A. Sanpera, G. V. Shlyapnikov, and M. Lewenstein, Phys. Rev. Lett. **83**, 5198 (1999).
[19] J. Denschlag, J. E. Simsarian, D. L. Feder, C. W. Clark, L. A. Collins, J. Cubizolles, L. Deng, E. W. Hagley, K. Helmerson, W. P. Reinhardt, S. L. Rolston, B. I. Schneider, and W. D. Phillips, Science **287**, 97 (2000).
[20] Z. Dutton, M. Budde, C. Slowe, and L. V. Hau, Science **293**, 663 (2001).
[21] G.-B. Jo, J.-H. Choi, C. A. Christensen, T. A. Pasquini, Y.-R. Lee, W. Ketterle, and D. E. Pritchard, Phys. Rev. Lett. **98**, 180401 (2007).
[22] P. Engels and C. Atherton, Phys. Rev. Lett. **99**, 160405 (2007).
[23] C. Becker, S. Stellmer, P. S. Panahi, S. Dörscher, M. Baumert, E.-M. Richter, J. Kronjäger, K. Bongs, and K. Sengstock, Nat. Phys. **4**, 496 (2008).
[24] J. J. Chang, P. Engels, and M. A. Hoefer, Phys. Rev. Lett. **101**, 170404 (2008).
[25] S. Stellmer, C. Becker, P. Soltan-Panahi, E.-M. Richter, S. Dörscher, M. Baumert, J. Kronjäger, K. Bongs, and K. Sengstock, Phys. Rev. Lett. **101**, 120406 (2008).
[26] A. Weller, J. P. Ronzheimer, C. Gross, J. Esteve, M. K. Oberthaler, D. J. Frantzeskakis, G. Theocharis, and P. G. Kevrekidis, Phys. Rev. Lett. **101**, 130401 (2008).
[27] P. O. Fedichev, A. E. Muryshev, and G. V. Shlyapnikov, Phys. Rev. A **60**, 3220 (1999).
[28] A. E. Muryshev, H. B. van Linden van den Heuvell, and G. V. Shlyapnikov, Phys. Rev. A **60**, R2665 (1999).
[29] Th. Busch and J. R. Anglin, Phys. Rev. Lett. **84**, 2298 (2000).
[30] G. Huang, J. Szeftel, and S. Zhu, Phys. Rev. A **65**, 053605 (2002).
[31] A. A. Svidzinsky and A. L. Fetter, Phys. Rev. Lett. **84**, 5919 (2000).
[32] A. A. Svidzinsky and A. L. Fetter, Phys. Rev. A **62**, 063617 (2000).
[33] E. Lundh and P. Ao, Phys. Rev. A **61**, 063612 (2000).
[34] J.-K. Kim and A. L. Fetter, Phys. Rev. A **70**, 043624 (2004).

[35] S. Middelkamp, P. G. Kevrekidis, D. J. Frantzeskakis, R. Carretero-González, and P. Schmelcher, Phys. Rev. A **82**, 013646 (2010).
[36] G. Lamporesi, S. Donadello, S. Serafini, F. Dalfovo, and C. Ferrari, Nat. Phys. **9**, 656 (2013).
[37] C. N. Weiler, T. W. Neely, D. R. Scherer, A. S. Bradley, M. J. Davis, and B. P. Anderson, Nature (London) **455**, 948 (2008).
[38] S. Middelkamp, P. J. Torres, P. G. Kevrekidis, D. J. Frantzeskakis, R. Carretero-González, P. Schmelcher, D. V. Freilich, and D. S. Hall, Phys. Rev. A **84**, 011605 (2011).
[39] T. Frisch, Y. Pomeau, and S. Rica, Phys. Rev. Lett. **69**, 1644 (1992).
[40] S. Inouye, S. Gupta, T. Rosenband, A. P. Chikkatur, A. Görlitz, T. L. Gustavson, A. E. Leanhardt, D. E. Pritchard, and W. Ketterle, Phys. Rev. Lett. **87**, 080402 (2001).
[41] V. Hakim, Phys. Rev. E **55**, 2835 (1997).
[42] N. G. Parker, N. P. Proukakis, M. Leadbeater, and C. S. Adams, Phys. Rev. Lett. **90**, 220401 (2003).
[43] N. G. Parker, N. P. Proukakis, C. F. Barenghi, and C. S. Adams, Phys. Rev. Lett. **92**, 160403 (2004).
[44] A. J. Allen, D. P. Jackson, C. F. Barenghi, and N. P. Proukakis, Phys. Rev. A **83**, 013613 (2011).
[45] N. G. Parker, A. J. Allen, C. F. Barenghi, and N. P. Proukakis, Phys. Rev. A **86**, 013631 (2012).
[46] G. Theocharis, P. G. Kevrekidis, M. K. Oberthaler, and D. J. Frantzeskakis, Phys. Rev. A **76**, 045601 (2007).
[47] Y. S. Kivshar and B. Luther-Davies, Phys. Rep. **298**, 81 (1998).
[48] D. L. Feder, M. S. Pindzola, L. A. Collins, B. I. Schneider, and C. W. Clark, Phys. Rev. A **62**, 053606 (2000).
[49] L. D. Carr, M. A. Leung, and W. P. Reinhardt, J. Phys. B **33**, 3983 (2000).
[50] N. S. Ginsberg, J. Brand, and L. V. Hau, Phys. Rev. Lett. **94**, 040403 (2005).
[51] J. Brand and W. P. Reinhardt, Phys. Rev. A **65**, 043612 (2002).
[52] S. Komineas and N. Papanicolaou, Phys. Rev. A **68**, 043617 (2003).
[53] M. Tylutki, S. Donadello, S. Serafini, L. P. Pitaevskii, F. Dalfovo, G. Lamporesi, and G. Ferrari, Eur. Phys. J. Spec. Top. **224**, 577 (2015).
[54] C. Becker, K. Sengstock, P. Schmelcher, P. G. Kevrekidis, and R. Carretero-González, New J. Phys. **15**, 113028 (2013).
[55] S. Donadello, S. Serafini, M. Tylutki, L. P. Pitaevskii, F. Dalfovo, G. Lamporesi, and G. Ferrari, Phys. Rev. Lett. **113**, 065302 (2014).
[56] M. J. H. Ku, W. Ji, B. Mukherjee, E. Guardado-Sanchez, L. W. Cheuk, T. Yefsah, and M. W. Zwierlein, Phys. Rev. Lett. **113**, 065301 (2014).
[57] A. Munoz Mateo and J. Brand, Phys. Rev. Lett. **113**, 255302 (2014).
[58] A. Görlitz, J. M. Vogels, A. E. Leanhardt, C. Raman, T. L. Gustavson, J. R. Abo-Shaeer, A. P. Chikkatur, S. Gupta, S. Inouye, T. Rosenband, and W. Ketterle, Phys. Rev. Lett. **87**, 130402 (2001).
[59] L. Salasnich, B. A. Malomed, and F. Toigo, Phys. Rev. A **76**, 063614 (2007).
[60] A. L. Fetter and A. A. Svidzinsky, J. Phys. Condens. Mater. **13**, R135 (2001).
[61] For high aspects ratios close to or within the solitonic vortex regime, the transverse position of the excitation is ill defined, and so only the axial position is evaluated.
[62] A. L. Fetter and J. K. Kim, J. Low Temp. Phys. **125**, 239 (2001).
[63] S. Serafini, M. Barbiero, M. Debortoli, S. Donadello, F. Larcher, F. Dalfovo, G. Lamporesi, and G. Ferrari, Phys. Rev. Lett. **115**, 170402 (2015).
[64] S. K. Schnelle, E. D. van Ooijen, M. J. Davis, N. R. Heckenberg, and H. Rubinsztein-Dunlop, Opt. Express **16**, 1405 (2008).
[65] C. F. Barenghi and N. G. Parker, in *A Primer on Quantum Fluids*, SpringerBriefs in Physics (Springer International Publishing, New York, 2016), pp. 84–89.
[66] M. Guilleumas and R. Graham, Phys. Rev. A **64**, 033607 (2001).
[67] M. C. Tsatsos, P. E. S. Tavares, A. Cidrim, A. R. Fritsch, M. A. Caracanhas, F. E. A. dos Santos, C. F. Barenghi, and V. S. Bagnato, Phys. Rep. **622**, 1 (2016).
[68] S. E. Weiner, M. C. Tsatsos, L. S. Cederbaum, and A. U. J. Lode, arXiv:1409.7670.
[69] M. C. Tsatsos and A. U. J. Lode, J. Low Temp. Phys. **181**, 171 (2015).
[70] K. Sakmann and M. Kasevich, Nat. Phys. **12**, 451 (2016).
[71] A. Minguzzi, S. Succi, F. Toschi, M. P. Tosi, and P. Vignolo, Phys. Rep. **395**, 223 (2004).
[72] A. U. J. Lode, M. C. Tsatsos, and E. Fasshauer, MCTDH-X, the time-dependent multiconfigurational Hartree for indistinguishable particles software, ultracold.org.